

MSEC2016-8837

RELATIVE ROBOTS: SCALING AUTOMATED ASSEMBLY OF DISCRETE CELLULAR LATTICES

Matthew Carney

The Center for Bits, and Atoms
Massachusetts Institute of Technology
Cambridge, Massachusetts 02139
Email: mcarney@mit.edu

Benjamin Jenett

The Center for Bits, and Atoms
Massachusetts Institute of Technology
Cambridge, Massachusetts 02139
Email: bej@mit.edu

ABSTRACT

We propose metrics for evaluating the performance of robotically assembled discrete cellular lattice structures (referred to as digital materials) by defining a set of tools used to evaluate how the assembly system impacts the achievable performance objective of relative stiffness. We show that mass-specific stiffness can be described by the dependencies $E^(\gamma, D(n, f, RA))$, where E^* is specific modulus, γ is lattice topology, and the allowable acceptance of the joint interface, D , is defined by an error budget analysis that incorporates the scale of the structure, and/or number of discrete components assembled, n , the type of robotic assembler, RA , and the static error contributions due to tolerance stack-up in the specified assembler structural loop, and the dynamic error limitations of the assembler operating at specified assembly rates, f . We refer to three primary physical robotic construction system topologies defined by the relationship between their configuration workspace, and the global configuration space: global robotic assembler (GR), mobile robotic assembler (MR), and relative robotic assemblers (RR), each exhibiting varying sensitivity to static, and dynamic error accumulation. Results of this analysis inform an iterative machine design process where final desired material performance is used to define robotic assembly system design parameters.*

INTRODUCTION

Digital materials exhibit coded functionality by programmatically defining the type, and location of homogeneous or heterogeneous discrete building blocks such that their mechanical

properties combine to perform as an explicitly defined continuum material. One example of a highly stiff, and ultra-light material is a high connectivity, non-stochastic, periodic, lattice structure composed of axially loaded truss elements [1]. Differentiating from 3D printing, discretization of the cellular lattice into reusable building-block elements enables fabrication, and reconfiguration, of explicitly defined heterogeneous meta-materials. The regular, periodic nature of the discrete cellular lattice can be exploited to simplify automated assembly by robotic processes. In this paper we lay out a methodology to identify the overall performance of robotic assembly of discrete cellular lattice with metrics based on machine class, scale of assembled material, and assembly rate. The critical dependency of robotic assembly is the ability for the interface between joined discrete cells (voxels) to accommodate error inherent to the assembly process while maintaining robust force/energy transfer across the node.

Performance of discrete construction of three dimensional periodic lattice structures is based on the behavior of cellular solids with properties governed by their constituent material, and lattice topology [2]. Analogous to naturally occurring cellular materials such as bone, and sponge, these engineered periodic lattices act as continuum meta-materials [3], which can achieve ultralight stiffness to weight ratios by following relative density linear scaling relationships from the base material to the lattice [4, 5].

In discrete lattice construction, the parasitic mass contribution of the interface affects overall system mass-specific stiffness. Given a base material with young's modulus E_s , and density ρ_s , ideal stretch dominated behavior with specific modulus

E^* at density ρ^* follows a proportional law of $\frac{E^*}{E_s} \propto \frac{\rho^*}{\rho_s}^\gamma$, where γ varies with lattice topology, and connectivity (Fig. 1) [3, 5]. In this paper, we will assume a single periodic cubic octahedra lattice topology with $\gamma = 1.5$.

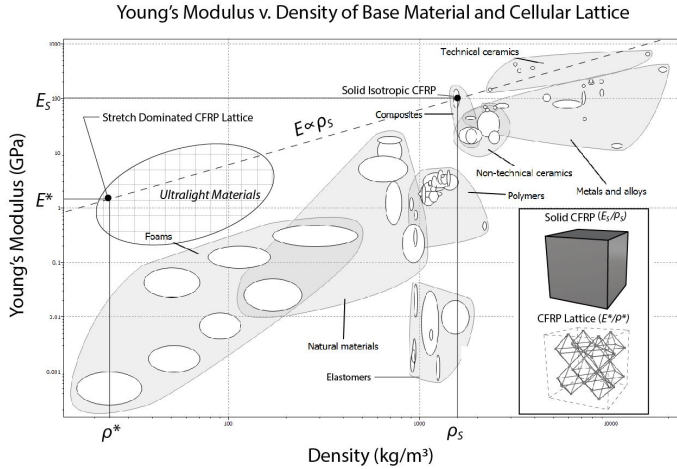


FIGURE 1. SPECIFIC MODULUS COMPARISON CHART.

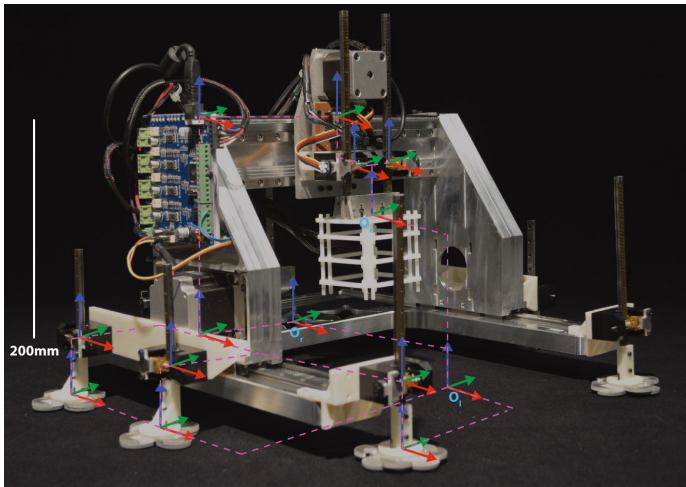


FIGURE 2. COORDINATE FRAMES OF MAJOR LINKS, and THEIR OFFSETS FOR AN HTM ANALYSIS OF THIS CUSTOM BUILT MR-TYPE ASSEMBLER. O_L IS THE BASE FRAME ORIGIN (LOCATED ON THE LATTICE), O_E IS THE TOOL FRAME.

Robotic assembly of truss structures has typically taken the form of multi-degree of freedom (DOF) industrial robot arms that place discrete truss segments into larger structural configurations [6]. In order to increase attainable build volume, linear stages are

built for the arm to translate around the structure it builds. Hoyt et al have developed an approach for on-orbit space assembly, using several multi-DOF arms to enable robot locomotion, truss manipulation, and assembly [7]. Terada et al have simplified the structure-robot system by designing the robot relative to the parts it places, unifying locomotion, and part placement [8].

We refer to three primary physical assembly system topologies that are defined by the relationship between their task-space, and global work-space coordinate frames: GR (global robotic assembler), MR (mobile robot), and RR (relative robot). Figure 2 shows a mobile robot, and Fig. 3 shows example assembly systems from each category.

Static, and dynamic error is accumulated differently in each machine class. Assembler static error is composed of constant, systematic structural loop tolerances due to machine kinematics, and manufacturing. The dynamic response of the assembly system to self, and forced-excitation defines a dynamic error contribution based on system configuration.

The speed at which parts can be placed, the build frequency (f), is a function of robot type (RR), and is defined by the interface geometry (D). The dynamics of the assembly robot contribute a vibrational error that decays toward a target position. The interface geometry accommodates the assembly system static, and dynamic error. The larger the allowable acceptance of the interface the shorter required settling time, resulting in increased allowable assembly rates.

Static error also accumulates in the incremental assembly of the lattice due to accumulated tolerance stack-up error of the assembled lattice elements. Each machine class exhibits varying sensitivity to this lattice tolerance stack-up, and plays a part in system choice. The combination of static, and dynamic errors defines a maximum positional variation at the interface (D) of the assembly front, and a minimum geometric interface condition to accommodate the positional tolerance. Larger tolerance management requirements grow the interface geometry, increasing interface node mass. Tighter tolerance assembly allows decreasing node interface geometry, which decreases mass, thereby increasing mass-specific stiffness.

We propose metrics for evaluating the performance of robotic assembly of discrete cellular lattices based on system error accumulation, mitigation of this by an allowable acceptance at the discrete interface, and those affects on material performance.

METHODOLOGY

We aim to define the dependencies of robotic assembly of discrete cellular lattice structures as a set of tools used to evaluate desired performance objectives. Specific stiffness, ultimately dependent on lattice topology (a factor that is a geometric constant), is affected by the mass of the mechanical interface between discrete voxels, as well as the mass of the lattice strut elements.

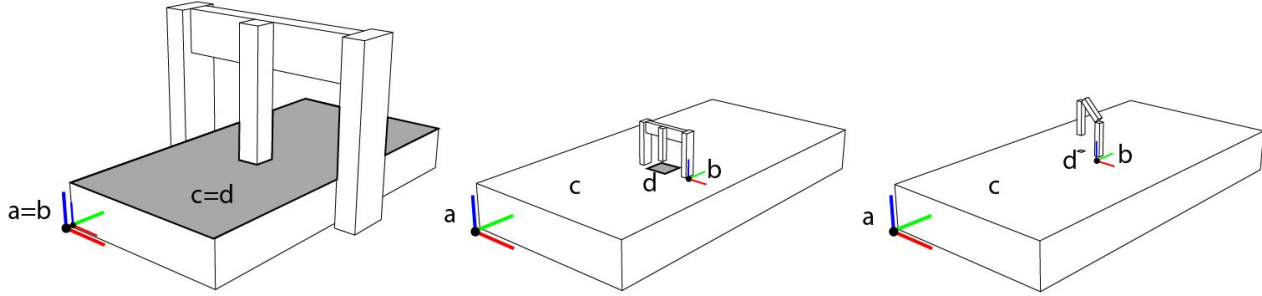


FIGURE 3. RELATIVE ROBOT CONFIGURATIONS (L TO R): GLOBAL (GR), MOBILE (MR), RELATIVE (RR). WHERE, a = GLOBAL COORDINATE FRAME, b = BASE FRAME, c = CONFIGURATION SPACE, d = WORK SPACE (SHADED REGIONS).

Geometric limitations of the interface geometry of the discrete cellular lattices are quantified by the type of robotic assembler, the number of discrete components assembled, the static error contributions due to tolerance stack-up in the assembler structural loop, and the dynamic error limitations due to assembly rate. This relationship is summarized with the following dependency:

$$E^*(\gamma, D(n, f, RA)) \quad (1)$$

E^* is the specific modulus of the assembled material, γ is a constant describing lattice topology, D is the interface geometry, n is number of parts composing the material (which can also be interpreted as scale of the overall geometry being built), f is part placement frequency, and RA refers to the type of robotic assembly system in use.

Equation 1 states that for an assembled material with a desired specific modulus there exists a geometrical limit to the voxel interface. The dimensions of this interface are based on the relationship between desired operating frequency, chosen assembly system, and the number of elements to be placed by a specified type of assembly robot. Ultimately, material performance is a function of each of the metrics shown in Eqn. 1. Each variable in this equation will now be described in greater detail.

Robotic Assembler Taxonomy (RA)

The robotic assemblers are categorized into three distinct system types defined by the relationship between their base frame, the global coordinate frame of the final assembled structure, and the assemblers configuration space [9]. A static datum at the origin of the lattice is defined for all system topologies as the global coordinate frame. The extents of the lattice (n voxel elements) define a global configuration space in \mathbb{R}^3 . Each robot class establishes a configuration(s) that can reach a subset of this configuration space defined by the kinematic limits of its workspace. The extents of the workspace are defined by the

number of units of voxels, m , that can be reached by the tool frame in a single configuration. The base frame of the global robotic assembler is static. The mobile assembly robots, having a workspace that is a subset of the configuration space must move across the lattice during the assembly process in order to reach the extents of structure. For each configuration these mobile robots establish new base frames relative to the global coordinate frame.

Global Robotic Assembler The global robotic assembler (GR) workspace reaches the full extents of the assembled structure ($m = n$). Since a single configuration is required for the tool frame to reach the entire workspace the base frame is aligned with the global coordinate frame. All motions of the end-effector tool frame are performed with respect to this static global reference [10]. We define such a machine as consisting of an analog motion system - a machine that can perform continuous, and arbitrary motions (dependent on its positional tolerance, and the kinematic limits of its drive system configuration) across the entire range of the assembled structure. During the assembly process voxels are placed with reference to this origin datum at the global coordinate frame. Generally a machine of this type is not mass or stiffness limited, thereby enabling high precision end-effector placement. However, the already assembled structure becomes part of the overall structural loop as voxels must interface with already placed components. As the assembly front approaches the further extents of the machine, tolerance stack-up of assembled components contribute to positional uncertainty at the target-voxel interface.

Mobile Robotic Assembler The mobile robotic assembler (MR) system is an assembly system that has similar kinematic configuration to a GR except the workspace is a subset of the total configuration space ($m < n$), and as such also includes a motion system to move across the lattice. In order to reach the extents of the configuration space the mobile assembler translates relative to the assembled lattice, establishing a new base coordinate frame after each locomotion maneuver to extend the

effective workspace of the tool frame. Similar to the GR, lattice elements contribute to the structural loop accumulating error. For the MR the structural loop consists of a reduced number of elements but includes additional structural components in the locomotion system.

Relative Robotic Assembler The relative robotic assembler system (RR) has a workspace that encompasses a minimal unit step ($m \simeq 1$). The kinematics are tuned to the geometry of the lattice, limiting motions to discrete or digital motions rather than analog continuous motions. Translation across the lattice is made in unit steps defined by the kinematics of this assembler. As the robot traverses the lattice it establishes a base coordinate frame at each step, places or removes an element, and then traverses to an adjacent cell, referencing only the previous, adjacent cell. In this way the tool frame is also the incrementally established base frame. This mobile relative robot minimizes the accumulation of error by reducing the structural loop to only neighboring elements, enabling the reference to be relative to the robot rather than the structure. The cost of this topology is complexity in locomotion, and material handling (not addressed here).

Scale (n)

While not explicitly an objective variable, scale (overall dimension or number of elements) of the assembled structure is a discerning factor in choosing a robotic assembly system. Assuming isotropic assembly (assembly in any principal direction), for n number of voxels with strut length L , the volume of assembled structure will have uniform x , y , and z dimensions of:

$$d = L\sqrt{2} \cdot \sqrt[3]{n} \quad (2)$$

This scaling will become important as we evaluate the consequences on robot selection for building very large scale structures where the extent of the material continuum surpasses a physically realizable machine enclosure size, and where the tolerance stack-up of placed parts becomes a substantial consideration.

Interface (D)

The interface joints between discrete lattice parts is the energy transfer point of the overall material; the interface may transmit force, moments, power, data, etc. This requires the geometry of the interface to accommodate docking of gendered features. The allowable acceptance of these features must accommodate the translational, and rotational errors of the assembly process, and provide passive alignment compensation in addition to energy transfer [11–13]. For simplicity of the discussion we consider only two dimensional interfaces with a single degree of freedom translational error - the approach direction is excluded

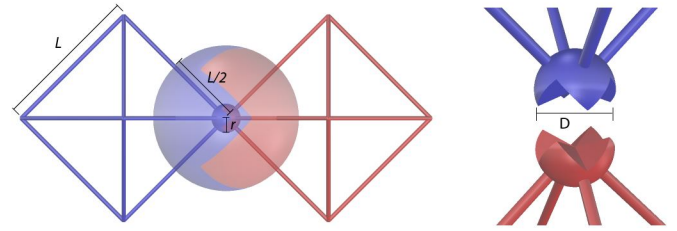


FIGURE 4. DISCRETE INTERFACE GEOMETRY. A) JOINT VOLUME CONTRIBUTION, B) ALLOWABLE ACCEPTANCE DIMENSION DEFINITION.

from the analysis. The acceptable allowance that the interface geometry must accommodate is then defined by the sum of static, and dynamic error contributions:

$$D = A + B + C \quad (3)$$

where, for the purposes of this paper we define the total error (D) as the sum of individual contributions from static lattice error (A), static assembler error (B), and dynamic assembler error (C). We exclude the dynamic response of the lattice due to the impact of placement, and locomotion - although, likely substantial it is beyond the scope of this paper.

The X-face interface described in [12] provides the maximum possible acceptable allowance for a 2D interface by enabling alignment with an offset equivalent to the entire width or height of a node. As such we make the assumption that D can be considered the minimum node diameter for successful alignment. When the dimensions of the node approach half the length of a strut, the cell is fully dominated by the node, and no strut remains. Evaluating the lattice as a cubic-octahedron cell type the maximum node size is then:

$$D_{max} = \frac{L}{\sqrt{2}} \quad (4)$$

Thus, for a given system configuration Eqn. 3 establishes a minimum node size. Applying this result to Eqn. 23 the maximum attainable specific modulus for a given assembly configuration can be determined.

Lattice Static Error Static error accumulates from the incremental addition of non-perfect elements to the lattice. When the elements contribute to the structural loop of the assembly process their error must be accounted for in the overall error budget analysis. This static lattice error contribution is defined by the error stack between the target orientation, and the assembler base

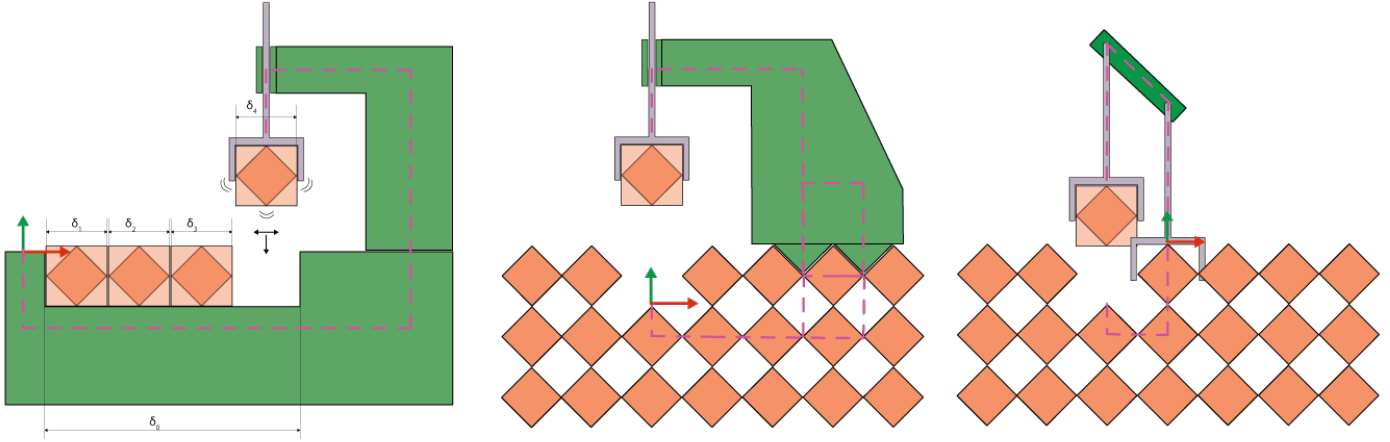


FIGURE 5. COORDINATE FRAME, and STATIC ERROR CONTRIBUTIONS FOR GR, MR, and RR TYPE ASSEMBLERS.

frame. The error contribution is incremental, and follows a traditional tolerance stack analysis. For the purposes of this analysis we utilize a root sum square weighting for the tolerance stack-up (ignoring 6σ manufacturing multipliers):

$$A = \left(\sum_{i=1}^N \sigma_i^2 \right)^{\frac{1}{2}} \quad (5)$$

where, σ_i is the manufacturing tolerance standard deviation of each voxel, N is the number of voxel cells in the structural loop. We specify A as the static error contribution of the lattice.

Assembler Static Error The assembler has a static systematic error contribution due to manufacturing, and assembly of the components in the structural loop described from its base reference frame to tool frame. The homogeneous transformation matrix (HTM) can be used to evaluate the amplifying effect of the relative translations, and rotations expressed through each link of the structure [14]. Each link, or subsystem has some nominal dimension, and with it some deviation from that nominal. The more parts that are assembled into the system, generally the larger the potential for error stack. Additionally, the longer the link lengths the more angular discrepancies can be amplified: this is known as *Abbe Error* [14]. Figure 2 shows a representation of the primary links on one half of a gantry-type mobile robotic assembler (MR) - the coordinate frames also mirror across the xz -plane. The task space of the end-effector is referenced to the work space origin of the assembly system. The homogeneous transformation matrix defines this relative relationship link-by-link:

$$\begin{bmatrix} X_R \\ Y_R \\ Z_R \\ 1 \end{bmatrix} = {}^R T_n \begin{bmatrix} X_n \\ Y_n \\ Z_n \\ 1 \end{bmatrix} \quad (6)$$

$${}^R T_n = \begin{bmatrix} O_{ix} & O_{iy} & O_{iz} & P_x \\ O_{jx} & O_{jy} & O_{jz} & P_y \\ O_{kx} & O_{ky} & O_{kz} & P_z \\ 0 & 0 & 0 & P_s \end{bmatrix} \quad (7)$$

The upper left quadrant defines angular orientation. The upper right column performs translations, while the P_s is a scaling factor (usually left as 1). The zeros are for the convenience of square matrix multiplication. The superscript, and subscript on the T are the reference, and current origin specifiers.

$$E_n = \begin{bmatrix} \varepsilon_{ix} & \varepsilon_{iy} & \varepsilon_{iz} & \delta_x \\ \varepsilon_{jx} & \varepsilon_{jy} & \varepsilon_{jz} & \delta_y \\ \varepsilon_{kx} & \varepsilon_{ky} & \varepsilon_{kz} & \delta_z \\ 0 & 0 & 0 & 1 \end{bmatrix} \quad (8)$$

The Eqn. 8 error transformation matrix is of the same form but with respect to deviations, and is added to each respective HTM. A total error budget analysis evaluates the incremental relative transformations along with the associated rotational, and translational errors. The total static error of the assembler is then the difference between the homogeneous transformation matrix, and

the total error budget analysis:

$$B = \prod_{m=1}^N m^{-1} T_m - \prod_{m=1}^N (m^{-1} T_m + m^{-1} E_m) \quad (9)$$

This assembler static error is machine specific, and systematic. In practice, precise metrology can be performed across the operational range of the assembly machine to identify, and map these errors. Mapped systematic errors can then be compensated for through machine control systems [14]. Alternatively, when available, manufacturer specifications can be utilized to estimate the overall static error range.

Assembler Dynamic Error Vibration due to the stiffness of the assembler contribute a dynamic error to the total acceptable error allowance. Self-excitation from gantry motion, and forced-excitation from part placement each contribute to dynamic error. A modal analysis results in a frequency response function that can be utilized to evaluate the lightly damped response of the assembler [15]. In order to perform this analysis the system is broken down into sub-assemblies characterized by masses, springs, and dampers. A lumped parameter analysis allows these sub-assemblies to be simplified into a single, second order system of equivalent mass, springs, and dampers [16].

$$\frac{d^2x}{dt^2} + \frac{c}{m} \frac{dx}{dt} + \frac{k}{m} (x + \delta) = \frac{f(t)}{m} \quad (10)$$

This second order system can then be evaluated in the frequency domain to identify system modal response. Then, applying a step input, and working back through the time domain we can solve for the settling time [17]: the time taken for the oscillatory behavior of the system to lose enough energy to be bounded by a specified error, δ , around a steady-state target value.

$$\begin{aligned} \frac{G(s)}{U(s)} &= \frac{\omega_n^2}{s^2 + 2\zeta\omega_n s + \omega_n^2} \\ \omega_n &= \sqrt{\frac{k}{m}} \\ \zeta &= \frac{c}{2m\omega_n} \end{aligned} \quad (11)$$

The analysis assumes a step input response to represent the assembly motion of displacing a cell by one cell width into position in the lattice. In classical controls the settling time of the end effector is specified for some allowable error range. In the case of lattice assembly we rearrange the settling time equation to evaluate what dynamic error range is to be expected for given system

dynamics, and desired assembly frequency.

$$t_s = \frac{-1}{\omega_n \zeta} \ln \frac{\delta}{u} \quad (12)$$

$$C = ue^{-t_s \omega_n \zeta} \quad (13)$$

where, t_s is settling time, ω_n is natural frequency, ζ is system damping, u is the step excitation input, and we define C as δ from Eqn. 12, the acceptable dynamic error range.

Total Error Budget The acceptable allowance that the interface geometry must accommodate is then defined by summation of each of the error contributions defined above: static lattice error (A), static assembler error (B), and dynamic assembler error (C). Equation 3 is repeated here for continuity.

$$\begin{aligned} D &= A + B + C \\ D &= \left(\sum_{i=1}^N \sigma_i^2 \right)^{\frac{1}{2}} + \prod_{m=1}^N m^{-1} T_m - \prod_{m=1}^N (m^{-1} T_m + m^{-1} E_m) + ue^{-t_s \omega_n \zeta} \end{aligned} \quad (14)$$

Equation 14 defines the gap that may exist between two nesting parts during placement that must be accommodated by passive mechanical features in the interface. The following section relates this gap size to the overall mass of the system, showing how the material specific stiffness is dependent on n , f , and l .

Specific Stiffness (E*)

The achievable specific elastic modulus of the cellular lattice structure effectively describes the performance of the assembled meta-material [2], and hence a specified lattice assembly system, which encapsulates both structure, and robotic assembly. Joints do not contribute to the overall stiffness of tension-dominated cellular structures [3], so it can be said that the joint is parasitic mass; a lower joint mass will result in a higher specific modulus. This may not be entirely the case in lower connectivity discrete lattices that rely on the joint interfaces to couple moments - this should be addressed in future research. For this paper we examine only the axially dominated load cases of a cubic-octahedron lattice where the modulus to density slope is $\gamma = 1.5$ [3].

To evaluate the performance of the lattice we examine the relative density of a single voxel (Fig. 6) using a volumetric representation of the joint as a function of strut length :

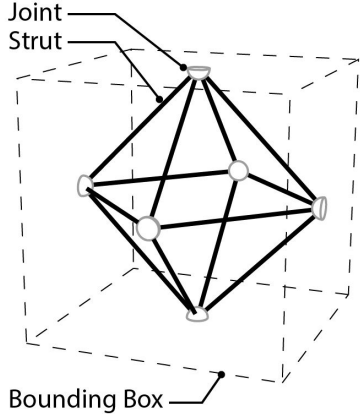


FIGURE 6. DISCRETE LATTICE VOXEL COMPONENT DEFINITION, and BOUNDING BOX.

$$\begin{aligned} d &= \frac{L}{30} \\ t &= \frac{L}{150} \end{aligned} \quad (15)$$

where, L is a given tubular strut length, with diameter d , and wall thickness t . For a tubular strut, the volume of material present is:

$$V_{strut} = \pi \left[\left(\frac{d}{2} \right)^2 - \left(\frac{d}{2} - t \right)^2 \right] \cdot L \quad (16)$$

$$V_{strut, total} = 12 \cdot V_{strut} \quad (17)$$

Next, we will determine the joint or interface volume, V_{joint} . The joint is represented as a sphere whose diameter is defined by the total error budget, D , determined from the previous section. Due to gender mirrored symmetry of the interface the volume of the joint is halved. The radius of the interface cannot extend beyond the mid-strut length $\frac{L}{\sqrt{2}}$, else the voxel is entirely dominated by interface geometry, and no strut remains - it becomes a solid cell.

$$V_{joint} = \frac{\frac{4}{3}\pi \left(\frac{\lambda D}{2} \right)^3}{2} \quad (18)$$

where, λ is a scaling factor necessary for geometric manufacturing considerations, which will be discussed in further publica-

tions. Total joint volume is:

$$V_{joint, total} = 6 \cdot V_{joint} \quad (19)$$

The total voxel volume is found by adding struts, and joints:

$$V_{voxel} = V_{joint, total} + V_{strut, total} \quad (20)$$

Then the voxel bounding box is determined according to Fig. 6:

$$V_{bounding} = \left(\frac{2L}{\sqrt{2}} \right)^3 \quad (21)$$

A commonly adopted method to evaluate the relative modulus was presented by [3]. The relative volume of a cell is proportional to the relative density. By finding a point on the specified relative modulus/density slope line of Fig. 1 we can identify the performance of the assembly system based on an achievable relative modulus. Nominally, the cellular solid is considered a lattice of struts with a specified cross-sectional area, and nodes, where the nodes have no additional mass other than the intersection of struts. In this case the following relationships are used:

$$\frac{\rho^*}{\rho_s} \propto \frac{E^*}{E_s} \propto \frac{V_{struts}}{V_{bounding}} \quad (22)$$

In discrete cellular lattice structures we require a modified method of evaluation that incorporates the additional mass due to the interface geometry at the joint. Joint mass (and volume) is non-structural in axial, tension-dominated structures. It is a volume necessary for the load transfer interface geometry but does not affect overall system stiffness; joint mass is, therefore, parasitic. The affect of joint volume is to lower the specific stiffness by shifting the lattice density higher while maintaining constant stiffness. Utilizing the modulus-density and proportional constants defined by [3] density-specific modulus of stretch-dominated lattices can be estimated by the following relations:

$$\rho_p^* = \frac{V_{struts} + V_{joints}}{V_{bounding}} \quad (23)$$

$$E^* \approx \frac{1}{3} E_s \left(\frac{\rho^*}{\rho_s} \right)^\gamma \quad (24)$$

where, E^* is the cellular lattice stiffness, ρ^* is the density of the nominal cellular lattice (no joints) ρ_p^* is parasitic cellular density, and the other subscripts are as defined previously. Finally, the density-specific, cellular stiffness is defined below.

$$E_{\rho}^* = \frac{E^*}{\rho_p^*} \quad (25)$$

This value provides a means to evaluate the parasitic contributions of joint interfaces, and ultimately to evaluate a full discrete cellular lattice robotic assembly system.

ANALYSIS

Applying the methodology described we evaluate the performance of three GR configurations across three orders of magnitude for scale, and speed, as well as one MR configuration that was built by the authors. Each configuration will use the same part type, with the following properties: $L= 70\text{mm}$, $d= 2.5\text{mm}$, $t= 0.5\text{mm}$, $\sigma = 0.1\text{mm}$.

Global Robotic Assembler

It should be noted that typical large format CNC gantry systems rarely exceed 10m as a free-spanning dimension. Therefore, for scales larger than 10m, we will assume the length is supported at 10m intervals in the longitudinal dimension, as is commonly seen with gantries with a longitudinal dimension on the order of 10^2m [18]. The resulting “linearized” geometries to be built are $1\text{m} \times 1\text{m} \times 1\text{m}$ (10^3 parts), $10\text{m} \times 10\text{m} \times 10\text{m}$ (10^6 parts), and $10\text{m} \times 10\text{m} \times 1000\text{m}$ (10^9 parts).

Calculation of Interface Tolerance Requirement

A. Lattice Static Error

10^3 parts:

Volume side length: 10 units = 1,000mm

$$A = \left(\sum_{i=1}^{10} 0.1^2 \right)^{\frac{1}{2}} = 0.32\text{mm} \quad (26)$$

10^6 parts:

Volume side length: 100 units = 10,000mm

$$A = \left(\sum_{i=1}^{100} 0.1^2 \right)^{\frac{1}{2}} = 1.0\text{mm} \quad (27)$$

10^9 parts:

Volume side length: 1000 units = 100,000mm

$$A = \left(\sum_{i=1}^{1000} 0.1^2 \right)^{\frac{1}{2}} = 3.2\text{mm} \quad (28)$$

B. Assembler Static Error Each length scale requires a specific gantry system, and these designs will reflect typical three axis CNC overhead gantry-type machining systems. For the GR case overall static error capabilities are published by the manufacturer, and used since direct measurements were not feasible to obtain.

GR-1: $B = 0.076 \text{ mm}$ [19]

GR-2: $B = 0.2 \text{ mm}$ [18]

GR-3: $B = 0.2 \text{ mm}$ [18]

C. Assembler Dynamic Error For this analysis damping is due to friction in the bolted connections between linkages, a assumed value of $\zeta = 0.05$ [20] is used, and for simplicity actuator damping, and stiffness is neglected. In order to estimate natural frequency we consider only the final link of the assembler, the end effector (Z axis), as a cantilevered beam. The stiffness, and mass of this link are defined by a beam of round cross section, and dimension given in Table 3.

$$C = ue^{-t_s \omega_n \zeta} \quad (29)$$

$$k_b = \frac{3EI}{L^3} \quad (30)$$

Where, for a round slender member, $d \ll L$. Inserting

$$\begin{aligned} \text{Area} &= \frac{\pi d^2}{4} \\ \text{Second Area Moment Inertia} &= \frac{\pi d^3}{64} \end{aligned} \quad (31)$$

into the stiffness equations we obtain a natural frequency for each of the GR cases, and evaluate their error response. The allowable error was chosen at a frequency equal to one tenth the system natural frequency to alleviate self excitation. The results of the analysis are shown in Table 1.

Mobile Robotic Assembler

The mobile robotic assembler shown in Fig. 2 was also evaluated. Immediately apparent is the static lattice error contribution is significantly reduced to just a few unit cells within the

RR	L [m]	d [m]	w_n [Hz]	$C (\frac{a_n}{10})$ [mm]
GR-1	0.5	0.1	3500	0.6
GR-2	5	1.0	3.5	0.6
GR-3	10	2.0	0.4	0.4

TABLE 1. DYNAMIC ERROR DUE TO ASSEMBLER CONFIGURATION

local configuration workspace, rather than the entire configuration space. Also significant is the additional complexity of the local locomotion system contributes to an increased assembler static error. The following analysis uses the methods described above.

A. Static Lattice Error The side length of the assembled structure is defined as 1000 units = 100,000mm. However, the mobile robot translates across the lattice structure, and in any configuration spans itself across only six voxel cell units. The static lattice error then only considers the error contribution of those voxels within the structural loop of the given assembler configuration.

10^9 parts:

Volume side length: 6 units = 600mm

$$A = \left(\sum_{i=1}^6 0.1^2 \right)^{\frac{1}{2}} = 0.28mm \quad (32)$$

B. Static Assembler Error A homogeneous transformation matrix, and error contribution budget analysis resulted in the following final error transformation matrix from the base frame to tool frame (angular error contributions were ignored for this analysis).

$${}^bT = \left[\begin{array}{ccc|c} 0.0 & 0.0 & 0.0 & 0.27 \\ 0.0 & 0.0 & 0.0 & 0.25 \\ 0.0 & 0.0 & 0.0 & 0.25 \\ \hline 0.0 & 0.0 & 0.0 & 0.0 \end{array} \right] \quad (33)$$

C. Dynamic Assembler Error The same operating frequency, and damping characteristics of the GR-1 test were used to evaluate the MR-1. The upper gantry beam was used as the sensitive component, and evaluated as an aluminum beam of cross sectional area 0.05m, and length 0.3m. The natural frequency of this system was found to be 5433 Hz. Evaluating an assembly rate of 10Hz, and 100Hz results in error contributions shown in Table 2.

RR	L [m]	d [m]	w_n [Hz]	C [mm]
MR-10	0.3	0.05	5400	1.5e-12
MR-100	0.3	0.05	5400	0.06

TABLE 2. DYNAMIC ERROR OF MR ASSEMBLER CONFIGURATION AT 10, and 100HZ ASSEMBLY RATES.

RR	A [mm]	B [mm]	C [mm]	D [mm]
GR-1	0.32	0.08	0.6	1.0
GR-2	1.0	0.2	0.6	1.8
GR-3	3.2	0.2	0.4	3.8
MR-10	0.28	0.27	1.5e-12	0.55
MR-100	0.28	0.27	0.06	0.61

TABLE 3. TOTAL ERROR BUDGET CONTRIBUTIONS

D. Total Mobile Robotic Assembler Error The total robotic assembler error contributions are laid out in Table 3. One distinction to make is the larger GR systems were evaluated at operating frequencies that were $\frac{1}{10}w_n$ where MR was instead evaluated at 10, and 100Hz ranges.

Specific Stiffness Calculation

Now that we have calculated varying values for D , we will show how to use this data to help determine ρ^* , and, more importantly, E^* . We will assume the material is carbon fiber reinforced plastic (CFRP, uniaxial pultruded, epoxy matrix), with a Young's Modulus $E = 100 GPa$, and a density $\rho = 1500 \frac{kg}{m^3}$.

Given a strut length $L = 70mm$, with a diameter $D = 2.5mm$, and a wall thickness $t = 0.5mm$, we can calculate the strut volume $V = 2.2 \times 10^{-7} m^3$, and the total strut volume is $12 * V = 2.64 \times 10^{-6} m^3$. This is considered the structural volume, from which we can calculate the structural mass $M = 3.96 \times 10^{-3} kg$. We calculate the bounding box volume to be $V_b = 9.7 \times 10^{-4} m^3$. We can then calculate the structural cellular density $\rho^* = 4.08 \frac{kg}{m^3}$. By following the slope $E \propto \rho^{1.5}$ to the calculated ρ^* , we can approximate the corresponding E^* to be around 0.01 GPa. As previously described, we can use the formula for the slope of the line to calculate the approximate value, which we find to be 0.014 GPa. This number represents the idealized cellular lattice composed of only structural mass. We can then evaluate the specific modulus $\frac{E^*}{\rho^*} = 3.48 * 10^{-3} GPa$.

We calculate the parasitic joint volume, and obtain a parasitic mass M_p , which is specific to each robotic system. This then allows evaluation of the penalty incurred by a larger mass

RR	$\rho_p^* [\frac{kg}{m^3}]$	$E_{s,p} [GPa]$
GR-1	4.24	$3.35 * 10^{-3}$
GR-2	4.42	$3.21 * 10^{-3}$
GR-3	5.42	$2.62 * 10^{-3}$
MR-10	4.17	$3.40 * 10^{-3}$
MR-100	4.18	$3.39 * 10^{-3}$

TABLE 4. COMBINED STRUCTURAL, and PARASITIC CELLULAR LATTICE DENSITY, and SPECIFIC MODULUS VALUES

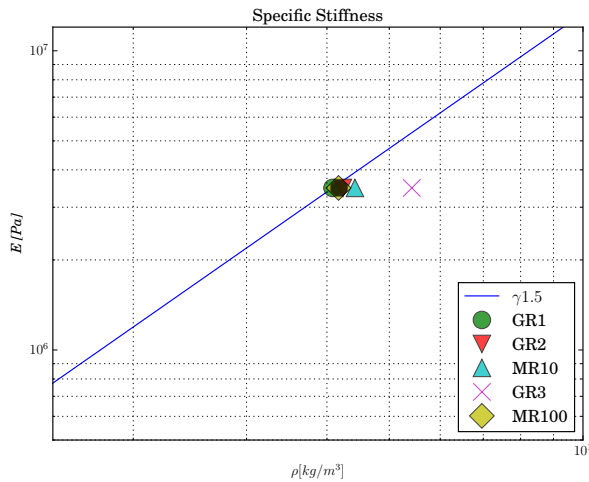


FIGURE 7. PARASITIC MASS DE-RATES THE STIFFNESS OF THE DISCRETE CELLULAR LATTICE, GIVING A LOWER SPECIFIC STIFFNESS THAN PREDICTED BY NOMINAL CELLULAR MATERIAL PROPORTIONS.

in a constant volume- higher parasitic density ρ_p^* for a constant stiffness, thus a lower specific parasitic stiffness $E_{s,p}$. These results are presented in Table 4, and Fig. 7 for the evaluated robotic systems.

DISCUSSION

Apparent from the analysis is that the GR assembly technique suffers on multiple metrics at increased scales. The static base frame is unable to accommodate the accumulation of error due to the static lattice tolerance error stack-up. What is most notable is that the stack-up of error due to the placement of parts is a significant contributor to the error, and ultimately the material performance. In contrast, systematic static assembler error can generally be compensated for by performing a system identification that maps error factors onto the operating workspace to

be compensated for through software control systems. The dynamic error is also comparable due to the ability for the machine design to accommodate significant mass, and in effect increased stiffness. In an effort to demonstrate major contributing factors of error the GR systems were evaluated each at $\frac{1}{10}w_n$, where MR were instead evaluated at 10, and 100Hz ranges. This discrepancy is to show the primary factors in the GR type system are due to A errors, while MR systems were used to show how dynamic errors, C, can contribute to error accumulation for otherwise constant machine parameters.

The results of this analysis shows that as scale increases a traditional GR system reaches a limit of functionality both due to tolerance management, as well the natural limit to the size of a machine that can be built. That said, there does exist a primary case where a GR system may be ideal: limited build scale with precision voxel components. This is where the high stiffness GR system enables assembly of cell types with small parasitic volume at the nodes. Robotic assembly systems that move relative to the structure are able to minimize the static error stack-up A. The MR configuration must still accommodate a static lattice error accumulation, though, the number of cells to accommodate in the structural loop is both a substantially limited subset of the global configuration space, and is a constant value of elements stacked within the extents of its analog motion system. The MR also exhibits, similar to the static assembler, B, error due to similar kinematics to the GR system. Not shown in the analysis but to be shown in further work, a RR system makes substantial wins with minimal static lattice error, reduced static assembler error due to simplified kinematics, and potentially reduced dynamic error due to decreased system extents.

CONCLUSION

We have presented a method of evaluating the performance of robotically assembled discrete cellular lattices by analysing the error contributions due to static, and dynamic errors from both the robotic assembler, and lattice structure. We have shown that high specific modulus materials can be assembled but the scale and frequency at which they are assembled may be limited by the type of robotic assembler used. In order to attain high specific stiffness at substantial scale it may be necessary to opt for the class of relative robots over traditional gantry-type systems. The methods outline the primary contributing factors of a first order error analysis, while further design iterations would provide detailed data for each of the error factors described. Further areas of research should include analysis of serial, and parallel error stack-up, effects of elasticity in the structure, and, the dynamics of the lattice.

ACKNOWLEDGMENT

This work was supported by NASA awards NNX14AG47A (Active Wing Shaping Control), and NNX14AH75A (Modular Rapidly Manufactured Spacecraft), and CBA sponsors.

REFERENCES

- [1] Cheung, K. C., and Gershenfeld, N., 2013. “Reversibly Assembled Cellular Composite Materials”. *Science*, **341**(6151), sep, pp. 1219–1221.
- [2] Gibson, L. J., and Ashby, M. F., 1999. *Cellular solids : structure and properties*. Cambridge solid state science series. Cambridge ; New York : Cambridge University Press, 1999.
- [3] Ashby, M. F., 2006. “The properties of foams and lattices.”. *Philosophical transactions. Series A, Mathematical, physical, and engineering sciences*, **364**(1838), jan, pp. 15–30.
- [4] Ashby, M. F., 2005. “Hybrids to fill holes in material property space”. *Philosophical Magazine*, **85**(26-27), sep, pp. 3235–3257.
- [5] Zheng, X., Lee, H., Weisgraber, T. H., Shusteff, M., DeOtte, J., Duoss, E. B., Kuntz, J. D., Biener, M. M., Ge, Q., Jackson, J. A., Kucheyev, S. O., Fang, N. X., and Spadaccini, C. M., 2014. “Ultralight, ultrastiff mechanical metamaterials.”. *Science (New York, N.Y.)*, **344**(6190), jun, pp. 1373–7.
- [6] Dorsey, J., Doggett, W., Hafley, R., Komendera, E., Correll, N., and King, B., 2012. “An Efficient and Versatile Means for Assembling and Manufacturing Systems in Space”. In AIAA SPACE 2012 Conference & Exposition, American Institute of Aeronautics and Astronautics.
- [7] Hoyt, R. P., Cushing, J. I., Slostad, J. T., Jimmerson, G., Moser, T., Kirkos, G., Jaster, M. L., and Voronka, N. R., 2013. SpiderFab : An Architecture for Self - Fabricating Space Systems.
- [8] Terada, Y., and Murata, S., 2004. “Automatic assembly system for a large-scale modular structure - hardware design of module and assembler robot”. In International Conference on Intelligent Robots and Systems, Vol. 3, IEEE/RSJ, pp. 2349–2355 vol.3.
- [9] Choset, H. M., 2005. *Principles of robot motion: theory, algorithms, and implementation*. Intelligent robotics and autonomous agents. Cambridge, Mass. : MIT Press, c2005.
- [10] Rudberg, T., 2013. “Increasing Machine Accuracy by Spatially Compensating Large Scale Machines for Use in Constructing Aerospace Structures”. *SAE International Journal of Aerospace*, **6**(1), sep, pp. 206–222.
- [11] Nilsson, Martin, 1999. “Symmetric Docking in 2D: A Bound on Self-Alignable Offsets”. pp. 7–11.
- [12] Eckenstein, N., and Yim, M., 2012. “The X-Face: An improved planar passive mechanical connector for modular self-reconfigurable robots”. In IEEE International Conference on Robotics and Systems, IEEE/RSJ, pp. 3073–3078.
- [13] Eckenstein, N., and Yim, M., 2014. “Area of acceptance for 3D self-aligning robotic connectors: Concepts, metrics, and designs”. In International Conference on Intelligent Robots and Automation, IEEE, pp. 1227–1233.
- [14] Slocum, A. H., 1992. *Precision machine design*. Dearborn, Michigan : Society of Manufacturing Engineers, c1992.
- [15] Schmitz, T. L., and Smith, K. S., 2009. *Machining dynamics: Frequency response to improved productivity*. Springer.
- [16] Koenigsberger, F., and Tlustý, J., 1970. *Machine tool structures*. Oxford, New York, Pergamon Press [c1970].
- [17] Nise, N. S., 2004. *Control systems engineering*. Hoboken, NJ : John Wiley, c2004.
- [18] EEW Protec, 2015. EEW-PROTEC GmbH: HSM-MODAL, dec.
- [19] Shopbot, 2015. PRSalpha CNC Routers, dec.
- [20] Asoor, A. A., and Pashaei, M. H., 2010. “Experimentally study on the effects of type of joint on damping”. *World applied sciences journal*, **8**(5), pp. 608–613.